ELSEVIER

15 September 1997

Optics Communications 141 (1997) 298–313

OPTICS COMMUNICATIONS

Full length article

The imaging of dielectric point scatterers in conventional and confocal polarisation microscopes

T. Wilson *, R. Juškaitis, P. Higdon

Department of Engineering Science, University of Oxford, Parks Road, Oxford OX1 3PJ, UK

Received 2 January 1997; revised 10 March 1997; accepted 9 April 1997

Abstract

We consider the image of a dielectric sub-resolution scatterer in conventional and confocal microscopes. We employ a vector theory and obtain theoretical images in a number of polarisation microscopes. In general the use of linear polarisation leads to asymmetric polarisation images whereas circularly symmetric polarisation images result if circular polarisation is used. Experimental results are presented to support the theoretical predictions. © 1997 Elsevier Science B.V.

1. Introduction

In its simplest form a conventional or confocal microscope may be converted into a polarisation instrument by inserting a polar into the illuminating beam and an analyser into the reflected (or transmitted) light path. The polar selects a particular, usually linear, polarisation which is then focussed by a high aperture microscope objective onto the specimen. The polarisation analyser is oriented so as to pass only light whose polarisation is orthogonal to that of the probe beam. The contrast which is generated provides useful information on specimen birefringence and dichroism in fields as diverse as crystallography [1] and biology [2].

However in certain applications the size of the features of interest are below the resolution limit of the microscope and in these cases the polarisation contrast is often due to the scattering properties of the features rather than their intrinsic optical anisotropy.

In order to enhance the contrast in polarisation microscopy it is desirable to reduce to a minimum the contribution to the image which arises from non-scattered light. It is usual to characterise this by an extinction ratio which is defined as the ratio of the intensity of light transmitted between parallel polars to that transmitted when the polars are crossed [3]. The measurements are taken in the absence of an object in a transmission system or in the presence of a perfect reflector in a reflection geometry. Ideally the extinction coefficient should be infinite. However the image formation properties of the conventional microscope prevent this even if the polars themselves are perfect [4,5] and typically a value of 10^3 is obtained. The coherent image formation in the confocal microscope, on the other hand, does permit an infinite extinction coefficient to be obtained [4]. In practice we have obtained values of the order of 1.5×10^5 which is close to the extinction ratio of our polarising elements alone. This suggests that the confocal polarisation microscope may have advantage over the conventional instrument even when imaging flat specimens.

This paper presents a theory of image formation in polarising microscopes by specialising to the case of a sub-resolution dielectric scatterer which might, for example, describe an impurity on the surface of a semiconductor specimen or a vesicle or other small element in biological tissue. Since we are concerned with polarisation effects we must abandon scalar theory and use vector theory to describe the components of the electric field at the focus of the microscope objective. These theories [6–8] are also not restricted to low numerical aperture systems. We will begin by describing the scattering properties of our dielectric particle and consider the form of the image in both

* Corresponding author. E-mail: tony.wilson@eng.ox.ac.uk.

PII S0030-4018(97)00226-5

conventional and confocal systems. The advantage of using circular polarisation will be considered and finally experimentally obtained images will be presented.

2. Theory

2.1. Preliminary considerations

In order to analyse the role played by small scattering particles on image contrast in scanning polarisation microscopy we consider the optical system of Fig. 1. The scatterer is assumed to be both illuminated and imaged by a high numerical aperture microscope objective. Our approach is to regard the illumination as an angular spectrum of plane waves in order to calculate the far field, $\boldsymbol{E}_1$, due to the scatterer. If we specialise to spherical particles the scattering problem may be solved analytically [9–11]. The far field, according to Mie theory, for a plane polarised incident wave is given in spherical polar co-ordinates as

$$\boldsymbol{E} = \cos\phi\, S_2(\cos\theta)\, \boldsymbol{i}_\theta - \sin\phi\, S_1(\cos\theta)\, \boldsymbol{i}_\phi, \qquad (1)$$

where $\boldsymbol{i}_\theta$ and $\boldsymbol{i}_\phi$ represent unit vectors in the θ and ϕ directions respectively. The functions S_1 and S_2 are determined by the size of the particle and its refractive index. Since our interest is in sub-resolution dielectric scatterers we may use a simplified form of Eq. (1). If we restrict ourselves to particles of radius a and refractive index μ_1 embedded in a medium of refractive index μ such that

$$x \ll 1, \quad |m|x \ll 1, \qquad (2)$$

where we have introduced the size parameter $x = 2\pi\mu a/\lambda$ where λ denotes the wavelength and the relative refractive index $m = \mu_1/\mu$. Under these circumstances the scattered far field is identical to that produced by an electric dipole whose dipole moment is proportional to the incident electric field [11]. If we denote the electric dipole moment by $\boldsymbol{p}$ then we can write the far field [12] as

$$\boldsymbol{E}_1 = -\boldsymbol{r} \wedge (\boldsymbol{r} \wedge \boldsymbol{p}). \qquad (3)$$

This expression also applies for sufficiently small particles regardless of their shape [13].

In order to proceed further it is necessary to describe the refraction of the scattered field by the lens. If we consider a component propagating in a direction whose unit vector is $\boldsymbol{r}$ then after refraction by the lens this component will be travelling parallel to the optic axis in the $\boldsymbol{k}$ direction. We resolve the scattered field, $\boldsymbol{E}_1$, into two components, one in the direction $\boldsymbol{r} \wedge \boldsymbol{k}$, which remains unchanged during refraction, and another in the direction $\boldsymbol{r} \wedge (\boldsymbol{r} \wedge \boldsymbol{k})$ which is rotated by refraction into the direction $\boldsymbol{k} \wedge (\boldsymbol{r} \wedge \boldsymbol{k})$. This permits us to write the scattered field $\boldsymbol{E}_2$, after refraction as

$$\left[(\boldsymbol{E}_1 \cdot \boldsymbol{r} \wedge \boldsymbol{k})(\boldsymbol{r} \wedge \boldsymbol{k}) + (\boldsymbol{E}_1 \cdot [\boldsymbol{r} \wedge (\boldsymbol{r} \wedge \boldsymbol{k})])\right.$$
$$\left.\times(\boldsymbol{k})\right](\boldsymbol{r} \wedge \boldsymbol{k})/[1 - (\boldsymbol{k} \cdot \boldsymbol{r}^2.$$

In the conventional scanning microscope this field is focussed down onto a large area detector. If we assume paraxial theory is valid in this region then the field at the detector is given by the Fourier transform of $\boldsymbol{E}_2$. Thus the intensity measured by an infinite detector is given, using Parceval's theorem, by

$$I_{\mathrm{conv}}(\rho_s, \phi_s) = \int_0^{2\pi}\int_0^{\alpha} |\boldsymbol{E}_2(\theta,\phi;\rho_s,\phi_s)\cdot\boldsymbol{n}|^2 \sin\theta \cos^{1/2}\theta \, \mathrm{d}\theta \, \mathrm{d}\phi, \qquad (5)$$

where ρ_s, ϕ_s represent the polar co-ordinates of the scan and the semi-angle α is determined by the numerical aperture of the objective lens. The factor $\cos^{1/2}\theta$ is included for objective lenses satisfying the aplanatic condi-

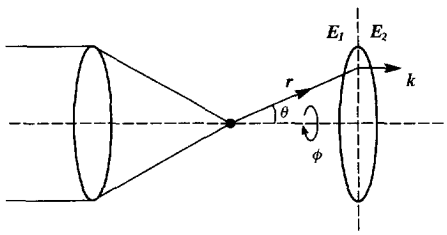

Fig. 1. Schematic diagram of the optical system.

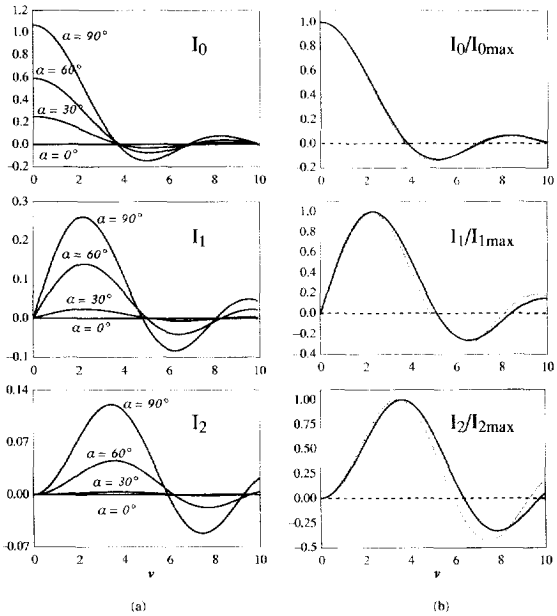

Fig. 2. The form of the functions $I_0(v,\alpha)$, $I_1(v,\alpha)$ and $I_2(v,\alpha)$ for a variety of values of α in (a). The normalised forms are shown in (b) where the two limiting values of $\alpha = 90°$ (feint line) and the small angle approximation of Eq. (10) (bold line) are compared.

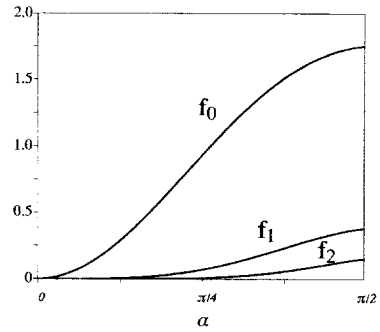

Fig. 3. The form of the functions $f_0(\alpha)$, $f_1(\alpha)$ and $f_2(\alpha)$ as a function of α.

tion [7]. Since we shall be concerned with polarisation imaging a vector, $\boldsymbol{n}$, has been included to describe the orientation of the polarisation analyser.

The confocal microscope, on the other hand, employs a point detector and so the image intensity in this case is given by the Fourier transform of $\boldsymbol{E}_2$, evaluated on-axis [14,15]. This gives an image intensity of

$$I_{\mathrm{conf}}(\rho_s,\phi_s) = \left| \int_0^{2\pi}\int_0^{\alpha} [\boldsymbol{E}_2(\theta,\phi;\rho_s,\phi_s)\cdot\boldsymbol{n}] \times \exp\{-jk\rho_s \sin\theta\cos(\phi-\phi_s)\} \sin\theta\cos^{1/2}\theta \,\mathrm{d}\theta\,\mathrm{d}\phi \right|^2, \quad (6)$$

where $k = 2\pi/\lambda$.

We note that Eqs. (5) and (6) imply that only the scattered field is present at the detectors. This is, of course, only true in a reflection geometry. In the transmission case the field is a superposition of the scattered and unscattered components. In a practical polarisation instrument the unscattered component is removed by a suitable crossed polar and so in the limit of our dipole-like scatterer Eqs. (5) and (6) apply equally in transmission and reflection.

It is now straightforward to calculate the conventional and confocal images once a suitable expression for the scattered far field, $\boldsymbol{E}_2$, has been determined. This may be obtained by substituting Eq. (3) into Eq. (4) to give

$$\begin{aligned}\boldsymbol{E}_2 = {} & \left\{ \frac{p_x}{2}[(1+\cos\theta) - (1-\cos\theta)\cos 2\phi] \right. \\ & \left. - \frac{p_y}{2}(1-\cos\theta)\sin 2\phi - p_z \sin\theta\cos\phi \right\} \boldsymbol{i} \\ & + \left\{ -\frac{p_x}{2}(1-\cos\theta)\sin 2\phi \right. \\ & \left. + \frac{p_y}{2}[(1+\cos\theta) + (1-\cos\theta)\cos 2\phi] \right. \\ & \left. - p_z \sin\theta\sin\phi \right\} \boldsymbol{j}, \end{aligned} \quad (7)$$

where p_x, p_y and p_z are the Cartesian components of the electric dipole moment and $\boldsymbol{i}$ and $\boldsymbol{j}$ are the unit vectors in x and y directions respectively. Since the particle is located at the focus of a high numerical aperture aplanatic microscope objective the dipole moment may be taken to be proportional to the electric field in the focal region [12]. The form of this field has been discussed in detail [6,7] and

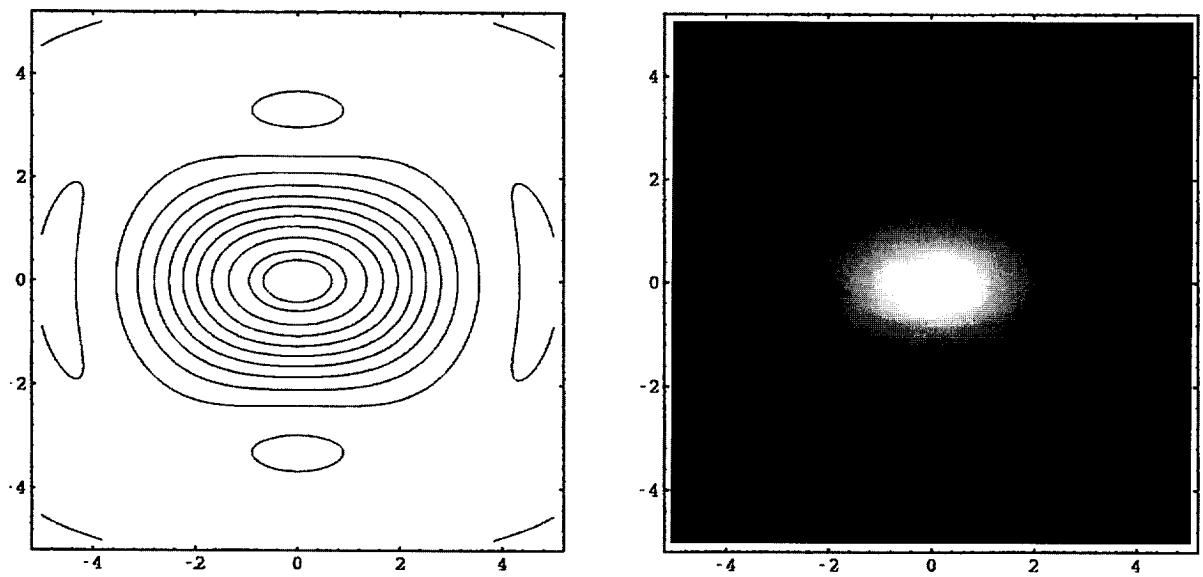

Fig. 4. The image of a dielectric scatterer in a conventional scanning microscope as both a contour plot and a density plot for the case of $\alpha = 90°$. The image is 10 optical units square and the contours are equally spaced between 0.05 and 0.95 and the intensity is normalised to unity on axis.

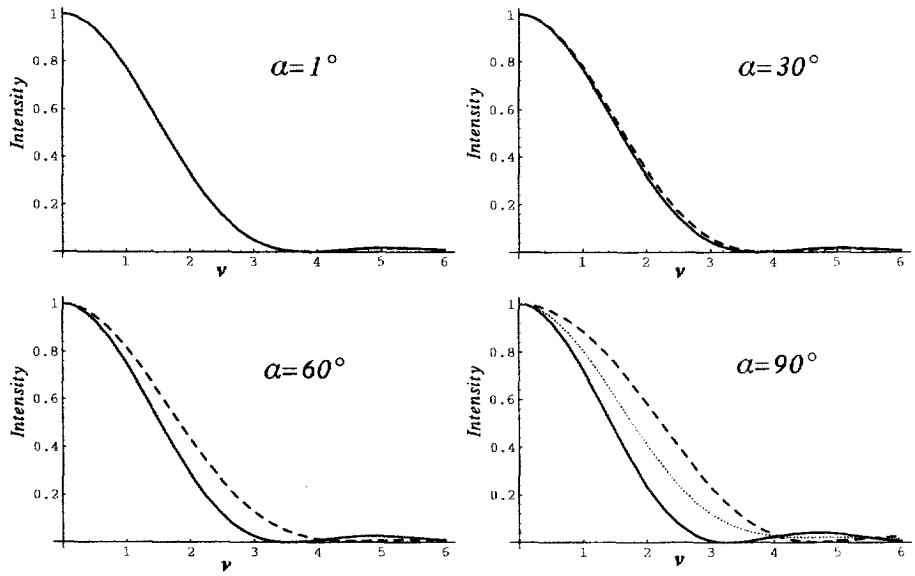

Fig. 5. The intensity in the image of a dielectric scatterer in a conventional microscope with equal aperture lenses. The dashed line corresponds to the intensity across the $\phi_s = 0$ radius whereas the full line corresponds to $\phi_s = 90°$. The dotted line on the $\alpha = 90°$ curves indicates the image intensity when circular polarisation is used.

for a plane wave polarised in the $\boldsymbol{i}$ direction incident on the objective lens we can write the dipole moment as

$$\boldsymbol{p} = \left(I_0(v,\alpha) + I_2(v,\alpha)\cos 2\phi_s \right) \boldsymbol{i} + I_2(v,\alpha)\sin 2\phi_s\, \boldsymbol{j} - 2\mathrm{j} I_1(v,\alpha)\cos\phi_s\, \boldsymbol{k}, \tag{8}$$

where the constant of proportionality has been omitted. The co-ordinate v is the optical co-ordinate corresponding to scan distance in the object plane ($v = k\rho_s \sin\alpha$). The integrals I_0, I_1, and I_2 are given [7] by

$$I_0(v,\alpha) = \int_0^{\alpha} \cos^{1/2}\theta \sin\theta\,(1+\cos\theta)\, J_0\!\left(\frac{v\sin\theta}{\sin\alpha}\right) \mathrm{d}\theta,$$

$$I_1(v,\alpha) = \int_0^{\alpha} \cos^{1/2}\theta \sin^2\theta\, J_1\!\left(\frac{v\sin\theta}{\sin\alpha}\right) \mathrm{d}\theta,$$

$$I_2(v,\alpha) = \int_0^{\alpha} \cos^{1/2}\theta \sin\theta\,(1-\cos\theta)\, J_2\!\left(\frac{v\sin\theta}{\sin\alpha}\right) \mathrm{d}\theta, \tag{9}$$

where $J_0(\ )$, $J_1(\ )$ and $J_2(\ )$ represent zero, first and second order Bessel functions of the first kind respectively. The form, and relative magnitudes, of these functions are shown in Fig. 2 where I_0 is seen to be much larger than I_1 and I_2 for small values of v. However the values of I_1 and I_2 become more significant as the angular aperture is increased. If each of the functions are normalised to, say, their maximum value it is found that their form does not depend strongly on the angular aperture, α, and so we may approximate them by their small α limiting expressions. The expressions are now easy to integrate and give

$$I_0(v,\alpha) \approx 2\alpha^2 \frac{J_1(v)}{v}, \quad I_1(v,\alpha) \approx \alpha^3 \frac{J_2(v)}{v},$$

$$I_2(v,\alpha) \approx \frac{\alpha^4}{2} \frac{J_3(v)}{v}. \tag{10}$$

These functions are also plotted in Fig. 2 in a normalised form and are seen to agree well with the directly computed values. The agreement in the $I_0(v,\alpha)$ case is particularly good.

2.2. Imaging in the conventional microscope

We begin by considering the image of our scatterer in the absence of any polarisation analysers. In this case Eq. (5) becomes

$$I_{\mathrm{conv}}(v,\phi_s) = \int_0^{2\pi}\int_0^{\alpha_2} |E_2|^2 \sin\theta \cos^{1/2}\theta\, \mathrm{d}\theta\, \mathrm{d}\phi, \tag{11}$$

where α_2 represents the angular aperture of the collector lens. This, together with Eq. (7), gives

$$I_{\mathrm{conv}}(v,\phi) = \left\{ |p_x|^2 + |p_y^2| \right\} \left\{ f_0(\alpha_2) + f_2(\alpha_2) \right\} + 4|p_z|^2 f_1(\alpha_2), \tag{12}$$

where the functions $f_0(\alpha)$, $f_1(\alpha)$ and $f_2(\alpha)$ are given by

$$f_0(\alpha) = \int_0^{\alpha} (1+\cos\theta)^2 \sin\theta \cos^{1/2}\theta\, \mathrm{d}\theta = \tfrac{2}{3}(1-\cos^{3/2}\alpha) + \tfrac{4}{5}(1-\cos^{5/2}\alpha) + \tfrac{2}{7}(1-\cos^{7/2}\alpha),$$

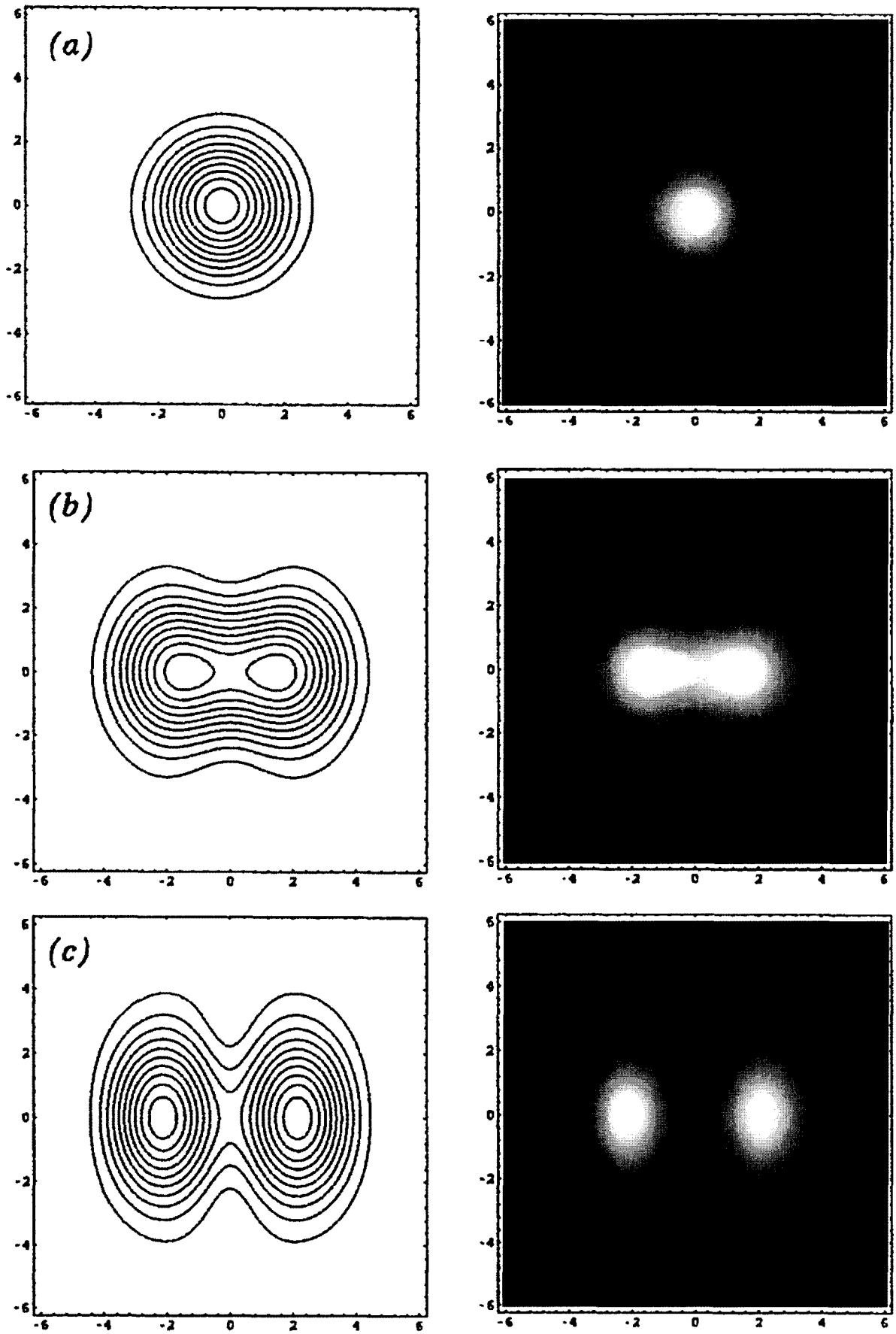
(a)
(b)
(c)

$$f_1(\alpha) = \int_0^{\alpha} \sin^2\theta \cos^{1/2}\theta \, d\theta$$
$$= \tfrac{2}{3}(1 - \cos^{3/2}\alpha) - \tfrac{2}{7}(1 - \cos^{7/2}\alpha),$$
$$f_2(\alpha) = \int_0^{\alpha} (1 - \cos\theta)^2 \sin\theta \cos^{1/2}\theta \, d\theta$$
$$= \tfrac{2}{3}(1 - \cos^{3/2}\alpha) - \tfrac{4}{5}(1 - \cos^{5/2}\alpha)$$
$$+ \tfrac{2}{7}(1 - \cos^{7/2}\alpha). \quad (13)$$

These functions are plotted in Fig. 3 and it is seen that, in general, $f_0(\alpha) > f_1(\alpha) > f_2(\alpha)$. If we now substitute expressions for p_x, p_y and p_z from Eq. (8) we obtain

$$I_{\text{conv}}(v,\phi_s) = \{I_0^2(v,\alpha_1) + 2I_0(v,\alpha_1)I_2(v,\alpha_1)\cos 2\phi_s$$
$$+ I_2^2(v,\alpha_1)\}\{f_0(\alpha_2) - f_2(\alpha_2)\}$$
$$+ 16I_1^2(v,\alpha_1)f_1(\alpha_2)\cos^2\phi_s, \quad (14)$$

where α_1 denotes the semi-angle of the illuminating objective lens. In general the image will be not circularly symmetric and Fig. 4 shows the extreme case corresponding to $\alpha = \alpha_1 = \alpha_2 = 90°$. Fig. 5 presents a comparison of

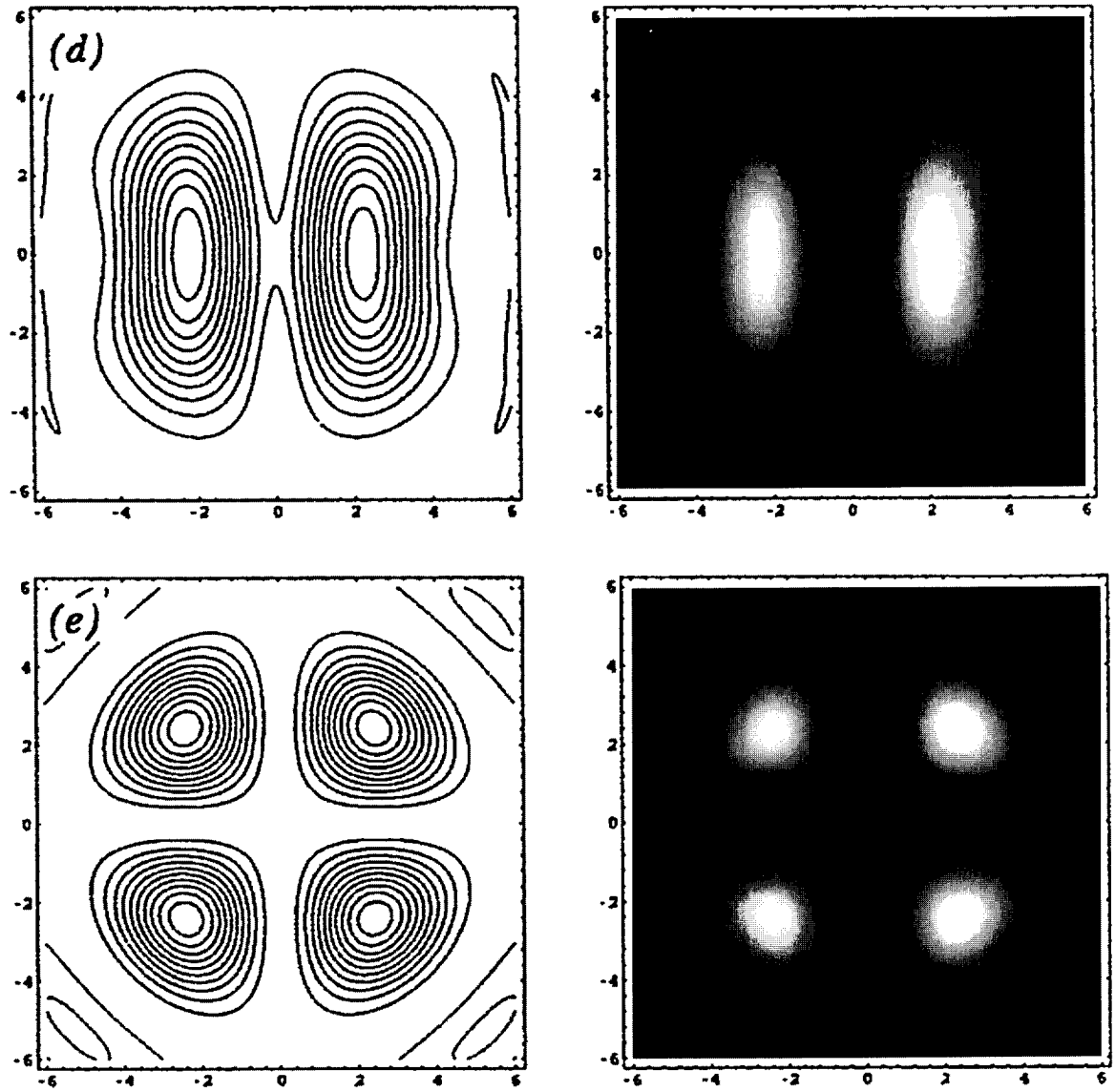

Fig. 6. The image of dielectric scatter when imaged between crossed linear polars for a variety of degrees of spatial coherence. (a), (c) Correspond to the incoherent and coherent limits respectively. The relative angular apertures are $\alpha_1 = 90°$, $\alpha_2 = 1°$ (a); $\alpha_1 = 60°$, $\alpha_2 = 30°$ (b); $\alpha_1 = \alpha_2 = 45°$ (c); $\alpha_1 = 30°$, $\alpha_2 = 60°$ (d) and $\alpha_1 = 1°$, $\alpha_2 = 90°$ (e). The images are twelve optical units square and the contours are equally spaced.

the intensity along $\phi_s = 0$ (dashed line) and $\phi_s = 90°$ (full line) as α increases. We see that the image is always narrower in the direction perpendicular to the incident polarisation but that the asymmetry is slight for all but the highest numerical apertures since for moderate values of α_1 the $I_0^2(v,\alpha_1)$ term tends to dominate the equation. Indeed for low numerical apertures the expression reduces to

$$I_{\text{conv}}(v) \sim I_0^2(v,\alpha_1) f_0(\alpha_2) \sim \left(\frac{2J_1(v)}{v}\right)^2, \tag{15}$$

which reproduces the Airy disc predicted by scalar theory [14].

If instead of using linearly polarised light we had chosen to use circularly polarised illumination then the field in the focal plane of the illuminating lens, and hence the dipole moment would take the form

$$\begin{aligned} \boldsymbol{p} = \frac{1}{\sqrt{2}}\{&[I_0(v,\alpha_1) + I_2(v,\alpha_1)\exp 2j\phi_s]\boldsymbol{i} \\ &+ j[I_0(v,\alpha_1) - I_2(v,\alpha_1)\exp 2j\phi_s]\boldsymbol{j} \\ &- 2jI_1(v,\alpha_1)\exp j\phi_s \boldsymbol{k}\}, \end{aligned} \tag{16}$$

which, with Eq. (12) leads to an image

$$\begin{aligned} I_{\text{conv}}(v) = &\{I_0^2(v,\alpha_1) + I_2^2(v,\alpha_1)\}[f_0(\alpha_2) + f_2(\alpha_2)] \\ &+ 8I_1^2(v,\alpha_1) f_1(\alpha_2), \end{aligned} \tag{17}$$

which is circularly symmetric for all values of α_1 and α_2 and again reduces to the Airy disc of Eq. (15) at low aperture. In general the image intensity lies between the full and dashed lines in Fig. 5. As an example the intensity corresponding to $\alpha = \alpha_1 = \alpha_2 = 90°$ is included in Fig. 5 as a dotted line.

Let us now consider the image of our scatterer between crossed polars. We begin by considering linearly polarised illumination of the objective and obtain the image intensity between crossed polars from Eqs. (5) and (8) with $\boldsymbol{n} = \boldsymbol{j}$ as

$$\begin{aligned} &I_{\text{conv}}(v,\phi_s) \\ &= \left(|p_x|^2 + |p_y|^2\right) f_2(\alpha_2) \\ &\quad + 2|p_y|^2 f_0(\alpha_2) + 4|p_z|^2 f_1(\alpha_2) \\ &= \{I_0(v,\alpha_1) + 2I_0(v,\alpha_1) I_2(v,\alpha_1)\cos 2\phi_s \\ &\quad + I_2^2(v,\alpha_1)\} f_2(\alpha_2) \\ &\quad + 2I_2^2(v,\alpha_1)\sin^2 2\phi_s f_0(\alpha_2) \\ &\quad + 16I_1^2(v,\alpha_1)\cos^2\phi_s f_1(\alpha_2). \end{aligned} \tag{18}$$

This is clearly quite a complicated image consisting of angularly dependent terms superimposed on a radially symmetric background. In order to obtain an idea of the relative importance of the three terms in Eq. (18) we may replace the functions of α with their low angle limiting forms. This leads, in the practically important case of $\alpha_1 = \alpha_2$ to

$$I_{\text{conv}}(v,\phi_s) \sim \left(\frac{J_2(v)}{v}\right)^2 \cos^2\phi_s, \tag{19}$$

which is zero along $\phi_s = \pm\pi/2$ and hence the image consists of two bright D-shaped regions. Fig. 6(c) shows the form of the image for the case of $\alpha_1 = \alpha_2 = 45°$. The general shape predicted by Eq. (19) remains but the intensity along $\phi_s = \pi/2$ is now a minimum rather than zero.

We note that in determining the relative strengths of the various terms in Eq. (18) we have assumed that objectives of equal aperture were used both to illuminate the object and to collect the scattered lights. If we now return to the general case we can again use the low angle approximations to obtain

$$\begin{aligned} I_{\text{conv}}(v) \sim &\left(\frac{J_1(v)}{v}\right)^2 \frac{\alpha_2^4}{5} + \left(\frac{J_3(v)}{v}\right)^2 \sin^2 2\phi_s\, \alpha_1^4 \\ &+ \frac{16}{3}\left(\frac{J_2(v)}{v}\right)^2 \cos^2\phi_s\, \alpha_1^2\alpha_2. \end{aligned} \tag{20}$$

As we have seen, if $\alpha_1 = \alpha_2$ the final term dominates. On the other hand in the incoherent limit ($\alpha_2 \gg \alpha_1$) the first term dominates and the image reverts to a circularly symmetric Airy disc. In the coherent limit ($\alpha_2 \ll \alpha_1$) the second term dominates and the image becomes

$$I_{\text{conv}}(v) \sim \left(\frac{J_3(v)}{v}\right)^2 \sin^2 2\phi_s, \tag{21}$$

which represents a four leaf clover pattern. We note that Burtin [6] obtained a similar result when considering the image of a small aperture in a screen between crossed polars in a conventional microscope. We show the transition between these various regions in Fig. 6 for a variety of combinations of α_1 and α_2 using the full expressions of Eq. (18).

We now finally return to the circularly polarised input case where the dipole moment is given by Eq. (16). If we elect to detect the orthogonal circular polarisation (by using a circular analyser consisting of a $\lambda/4$ plate and linear polariser) the image becomes

$$\begin{aligned} I_{\text{conv}}(v) \sim &I_2^2(v,\alpha_1) f_0(\alpha_2) + I_0^2(v,\alpha_1) f_2(\alpha_2) \\ &+ 8I_1^2(v,\alpha_1) f_1(\alpha_2), \end{aligned} \tag{22}$$

which, as expected, is circularly symmetric. We can again see the importance of the various terms by introducing their low angle approximations

$$\begin{aligned} I_{\text{conv}}(v) \sim &\left(\frac{J_3(v)}{v}\right)^2 \frac{\alpha_1^4}{2} + \left(\frac{J_1(v)}{v}\right)^2 \frac{\alpha_2^4}{5} \\ &+ \frac{8}{3}\left(\frac{J_2(v)}{v}\right)^2 \alpha_2\alpha_1^2. \end{aligned} \tag{23}$$

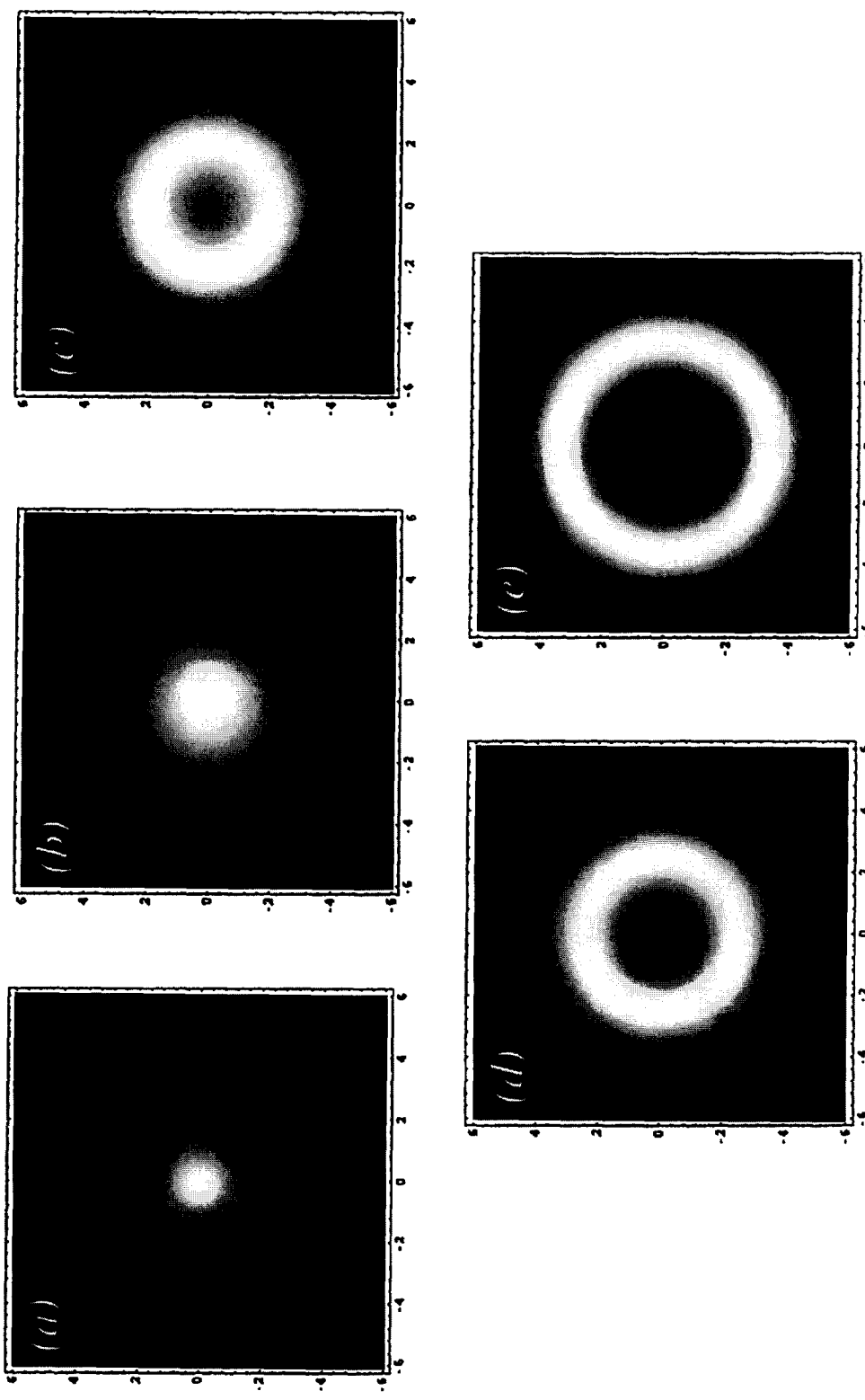

Fig. 7. The crossed-polar image of image of a dielectric scatterer using circularly polarised light. The relative angular apertures of the microscope objectives are $\alpha_1 = 90°$. $\alpha_2 = 1°$ (a); $\alpha_1 = 60°$, $\alpha_2 = 30°$ (b); $\alpha_1 = \alpha_2 = 45°$ (c); $\alpha_1 = 30°$, $\alpha_2 = 60°$ (d) and $\alpha_1 = 1°$, $\alpha_2 = 90°$ (e).

Again we see that when $\alpha_1 = \alpha_2$ the third term dominates and the image takes the form of a circular doughnut $(J_2(v)/v)^2$. In the incoherent limit, $\alpha_2 \gg \alpha_1$, a regular Airy disc results whereas in the coherent limit, $\alpha_2 \ll \alpha_1$, another doughnut image results, but this time given by $(J_3(v)/v)^2$. Fig. 7 shows the form of the images calculated from Eq. (22).

2.3. Imaging in the confocal microscope

Again we begin by considering the image of the point scatterer in the absence of a polarisation analyser. Eq. (6) becomes

$$I_{\text{conf}} = \left| \int_0^{2\pi} \int_0^{\alpha} \boldsymbol{E}_2(\theta,\phi) \exp\{-\mathrm{j}k\rho_s \sin\theta \cos(\phi - \phi_s)\} \times \sin\theta \cos^{1/2}\theta \, \mathrm{d}\theta \, \mathrm{d}\phi \right|^2 . \tag{24}$$

The form of $\boldsymbol{E}_2$ is given by Eq. (7). The integrals in ϕ may be readily performed by noting [7]

$$\int_0^{2\pi} \begin{matrix} \cos n\phi \\ \sin n\phi \end{matrix} \exp\{\mathrm{j}a\cos(\phi - \phi_s)\} \, \mathrm{d}\phi = 2\pi(\mathrm{j})^n J_n(a) \begin{matrix} \cos n\phi_s \\ \sin n\phi_s \end{matrix}, \tag{25}$$

which, together with the functions defined in Eq. (9) permit the integrals in Eq. (24) to be performed and to give the confocal image field, $\boldsymbol{E}_{\text{conf}}$, as

$$\begin{aligned} \boldsymbol{E}_{\text{conf}} = {} & \left[p_x \{ I_0(v,\alpha_2) + I_2(v,\alpha_2)\cos 2\phi_s \} \right. \\ & + p_y I_2(v,\alpha_2) \sin 2\phi_s + 2\mathrm{j} p_z I_1(v,\alpha_2) \cos\phi_s \left. \right] \boldsymbol{i} \\ & + \left[p_x I_2(v,\alpha_2) \sin 2\phi_s + p_y \{ I_0(v,\alpha_2) \right. \\ & \left. - I_2(v,\alpha_2)\cos 2\phi_s \} + 2\mathrm{j} p_z I_1(v,\alpha_2) \sin\phi_s \right] \boldsymbol{j}. \end{aligned} \tag{26}$$

Since the imaging in confocal microscopes is always coherent and the systems usually image in reflection we shall specialise to the case of $\alpha_1 = \alpha_2 = \alpha$ which, together with Eq. (8) permits us to write

$$\begin{aligned} \boldsymbol{E}_{\text{conf}} = {} & \left\{ I_0^2(v,\alpha) + 2I_1^2(v,\alpha) + I_2^2(v,\alpha) \right. \\ & \left. + 2\left[I_0(v,\alpha) I_2(v,\alpha) + I_1^2(v,\alpha) \right] \cos 2\phi_s \right\} \boldsymbol{i} \\ & + 2\left[I_0(v,\alpha) I_2(v,\alpha) + I_1^2(v,\alpha) \right] \sin 2\phi_s \, \boldsymbol{j}. \end{aligned} \tag{27}$$

The confocal image in the absence of a polarisation analyser is simply given by the modulus square of this expression which will again exhibit a small asymmetry at high apertures. Fig. 8 shows the limiting case of $\alpha = 90°$ and, as in the conventional case, the image is sharper in the direction perpendicular to the direction of polarisation of the incident light. We also see that the image in the confocal microscope is sharper than that in the conventional instrument, Fig. 4. The asymmetry in the image is, of course, a function of the angular aperture, α, and Fig. 9 demonstrates this by comparing the intensity across the $\phi_s = 0$ radius (dashed line) with that across the $\phi_s = 90°$, (full lines) and we see, as in the conventional case, that only at the highest aperture is the asymmetry likely to be

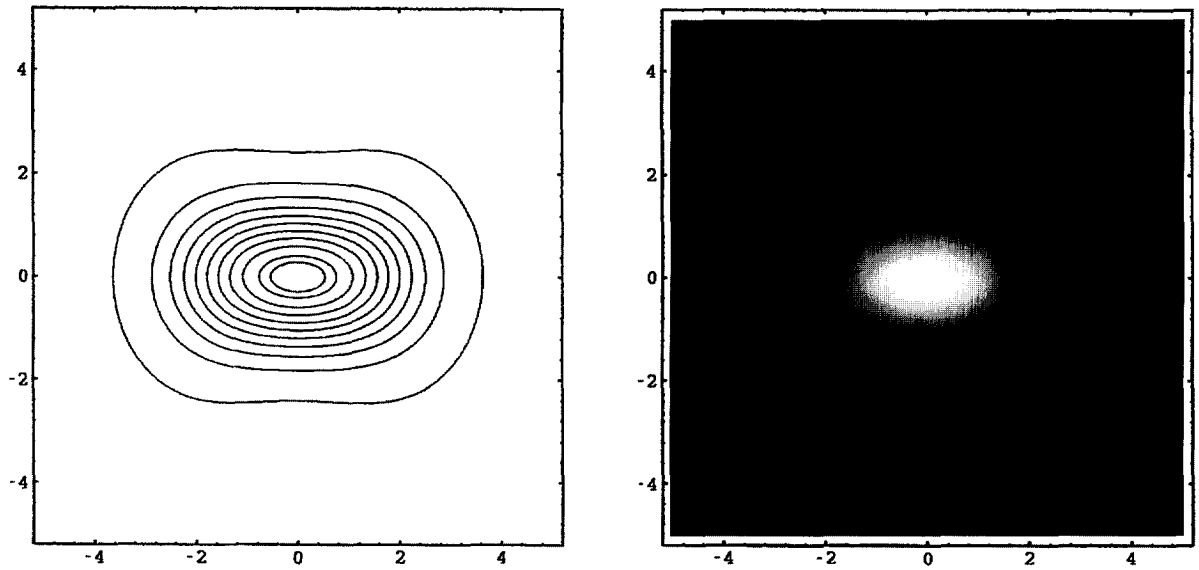

Fig. 8. The image of a dielectric scatterer in a confocal microscope. The image size is ten optical units square and the images correspond to an angular aperture, α, of 90°. The contours are equally spaced from 0.05 to 0.95 and the intensity is normalised to unit on-axis.

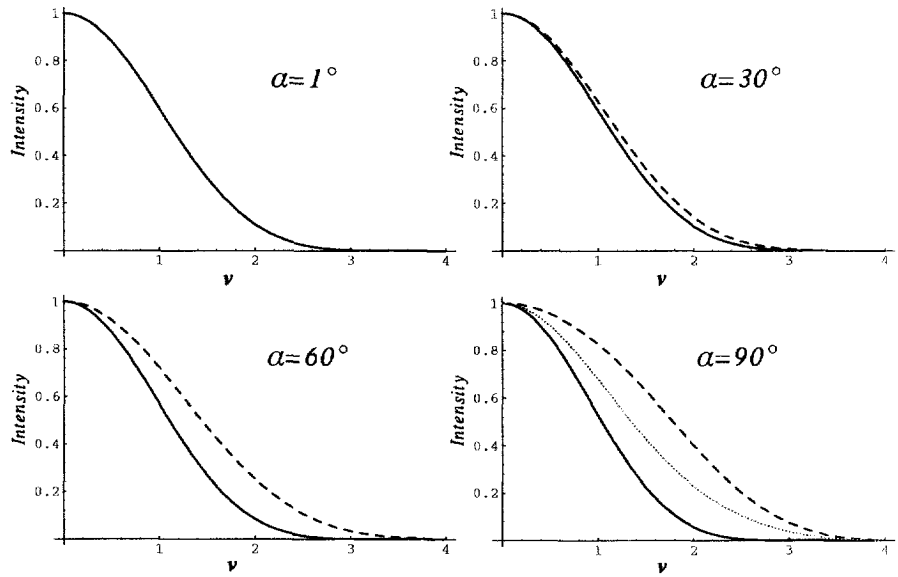

Fig. 9. The intensity in the image of a dielectric scatterer in a confocal microscope with equal aperture lenses, the dashed line corresponds to the intensity across the $\phi_s = 0$ radius whereas the full line corresponds to the $\phi_s = 90°$ radius. The dotted line on the $\alpha = 90°$ curves show the image intensity when circular polarisation is used.

noticeable in practice. We note that at lower apertures the $I_0(v,\alpha)$ term dominates the expressions and hence

$$I_{\text{conf}}(v) \sim I_0^4(v,\alpha) \sim \left(\frac{2J_1(v)}{v}\right)^4, \tag{28}$$

which agrees with the predictions of previous scalar theories [14]. The asymmetry in the image is removed if the objective lens is illuminated with circularly polarised light. In this case the dipole moments are given by Eq. (16) which leads to

$$I_{\text{conf}}(v) = \left[I_0^2(v,\alpha) + 2I_1^2(v,\alpha) + I_2^2(v,\alpha)\right]^2 + 4\left[I_0(v,\alpha)\, I_2(v,\alpha) + I_1^2(v,\alpha)\right]^2, \tag{29}$$

which, as expected is radially symmetric. In general this

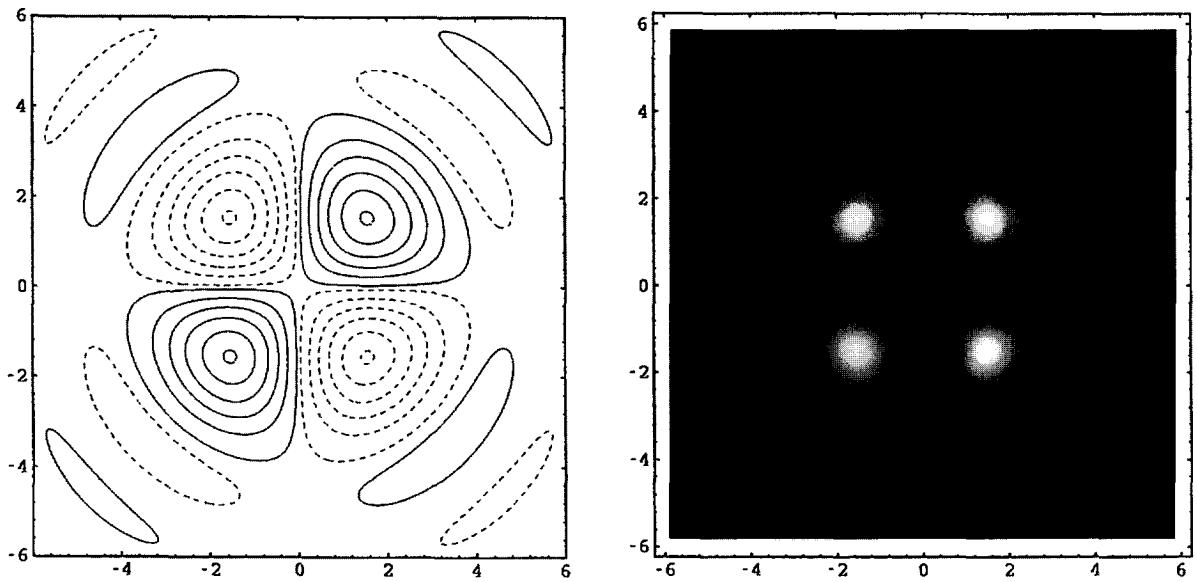

Fig. 10. The image of a dielectric scatterer between crossed polars in a confocal microscope. The density plot shows the image intensity whereas the contour plot shows the image field. The dashed contours represent negative values. The image in both cases is twelve optical units square and corresponds to an angular aperture of 60°.

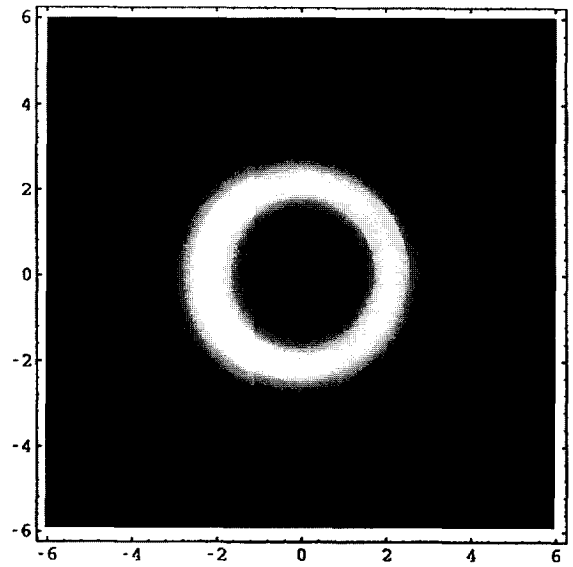

Fig. 11. The crossed polar image of a dielectric scatterer in a confocal microscope using circularly polarised light. The image is twelve optical units square and corresponds to an angular aperture of 60°.

function lies between the $\phi_s = 0°$ and $\phi_s = 90°$ curves in Fig. 9 and, as an example, the curve is super-imposed on the $\alpha = 90°$ curves in Fig. 9 as a dotted line.

If we now return to plane polarised illumination of the objective lens it is easy to see from Eq. (27) that the image between crossed polars is given by

$$E_{\text{conf}}(v,\phi_s) \sim \left[I_0(v,\alpha)\, I_2(v,\alpha) + I_1^2(v,\alpha) \right] \sin 2\phi_s. \tag{30}$$

Fig. 10 shows the intensity, $|E_{\text{conf}}(v,\phi_s)|^2$, as a density plot which reveals a four leaf clover pattern. We note that the symmetry of this image is identical to that found in the coherent limit of the conventional microscope, Eq. (21). We also show, in Fig. 10, a contour plot of the field, $E_{\text{conf}}(v,\phi_s)$, to emphasize the change of sign between adjacent quadrants. This has implications for the imaging of line structures and predicts that features running parallel or perpendicular to the incident polarisation direction will not be imaged efficiently [4]. In the case of "crossed circular" polarisation the image field becomes

$$E_{\text{conf}}(v) = \left[I_0(v,\alpha)\, I_2(v,\alpha) + I_1^2(v,\alpha) \right] \exp j2\phi_s, \tag{31}$$

and the image $|\boldsymbol{E}_{\text{conf}}(v)|^2$ is circularly symmetric and again has the form of a doughnut, Fig. 11.

Although a transmission system was shown in Fig. 1 the results obtained apply equally to an in-focus reflection system. If defocus is present, however, the transmission and reflection systems behave differently and we must differentiate carefully between them. In order to include the effects of defocus, z, it is necessary to modify the definitions of $I_0(v,\alpha)$, $I_1(v,\alpha)$ and $I_2(v,\alpha)$ in Eq. (9), which are used to describe the field on the focal region of a microscope objective [7], to

$$\begin{aligned} I_0(v,\alpha) &= \int_0^{\alpha} \cos^{1/2}\theta \sin\theta\,(1+\cos\theta)\, J_0\!\left(\frac{v\sin\theta}{\sin\alpha}\right) \\ &\quad \times \exp(jkz\cos\theta)\, d\theta, \\ I_1(v,\alpha) &= \int_0^{\alpha} \cos^{1/2}\theta \sin^2\theta\, J_1\!\left(\frac{v\sin\theta}{\sin\alpha}\right) \\ &\quad \times \exp(jkz\cos\theta)\, d\theta, \\ I_2(v,\alpha) &= \int_0^{\alpha} \cos^{1/2}\theta \sin\theta\,(1-\cos\theta)\, J_2\!\left(\frac{v\sin\theta}{\sin\alpha}\right) \\ &\quad \times \exp(jkz\cos\theta)\, d\theta. \end{aligned} \tag{32}$$

The confocal image field is still given by Eq. (26) but now the values of $I_0(v,\alpha)$, $I_1(v,\alpha)$ and $I_2(v,\alpha)$ in the expressions for the dipole moment, $\boldsymbol{p}$, are determined by the focus of the illuminating lens whereas the other values of $I_0(v,\alpha)$, $I_1(v,\alpha)$ and $I_2(v,\alpha)$ in Eq. (26) correspond to the focus of the collector lens. In a reflection system the defocus of both lenses is equal and hence all our previous equations apply unchanged except that $I_0(v,\alpha)$, $I_1(v,\alpha)$ and $I_2(v,\alpha)$ are now given by Eq. (32) rather than Eq. (9). In transmission, on the other hand, the defocus of the

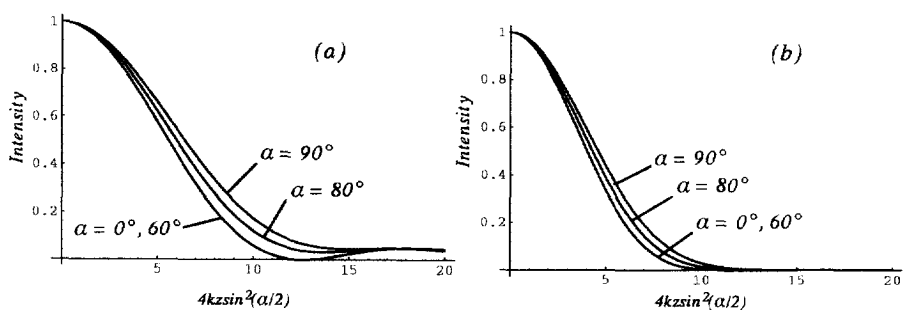

Fig. 12. The variation in intensity along the optic axis in the image of a dielectric scatterer for (a) convention and (b) confocal microscopes.

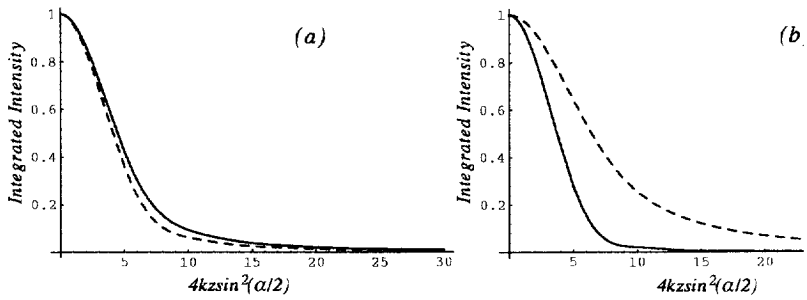

Fig. 13. The integrated intensity as a function of defocus, z for reflection (dashed line) and transmission (fu
$\alpha = 60°$. The curves in (a) represent brightfield imaging while those in (b) correspond to imaging between cr

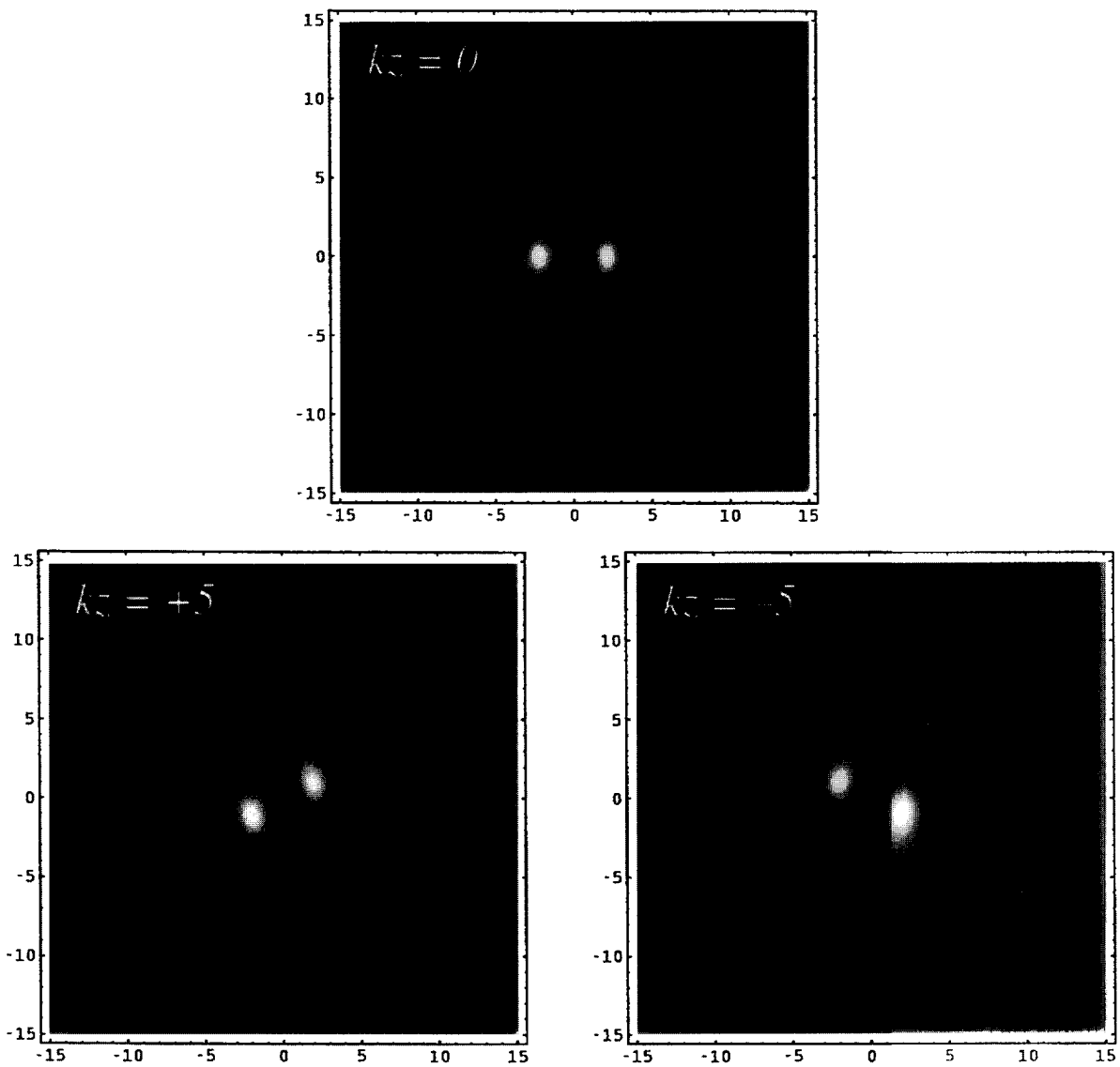

Fig. 14. The interference image between crossed circular polars for the case of $\alpha = 60°$ for zero defocus and equal and opposite defocus, $kz = \pm 5$. The image area is 30 optical units square.

lenses is equal and opposite and hence the confocal image field becomes

$$E_{\mathrm{conf}}(v,\phi_s) = \left[|I_0(v,\alpha)|^2 + 2|I_1(v,\alpha)|^2 + |I_2(v,\alpha)|^2 + 2\left(\mathrm{Re}\{I_0(v,\alpha)\, I_2^*(v,\alpha)\} + |I_1(v,\alpha)|^2\right)\cos 2\phi_s\right] i + 2\left[\mathrm{Re}\{I_0(v,\alpha)\, I_2^*(v,\alpha)\} + |I_1(v,\alpha)|^2\right]\sin 2\phi_s\, j, \tag{33}$$

which is always real and is fundamentally different in form from Eq. (27) which describes the reflection case. The two expressions are, of course, identical in the absence of defocus. If we consider the intensity on axis ($v = 0$) then the two expressions are again equal and are given by, in the absence of polars as,

$$I_{\mathrm{conf}}(z) = |I_0(0,\alpha)|^4, \tag{34}$$

which may be evaluated analytically in terms of Fresnel integrals. Fig. 12 shows the form of this image where we see that an increase in aperture widens the response. We also show the image in a conventional microscope for comparison.

A useful measure of the optical sectioning property of the confocal microscope is the integrated intensity which is essentially a measure of the energy in a particular plane as a function of defocus. It is given by

$$I_{\mathrm{int}}(z) = \int_0^{\infty}\int_0^{2\pi} I_{\mathrm{conf}}(v,\phi_s)\, v\, \mathrm{d}v\, \mathrm{d}\phi_s, \tag{35}$$

which, in the absence of polars, is given in a reflection system by

$$I_{\mathrm{int}} = \int_0^{\infty}\left\{|I_0^2(v,\alpha) + 2I_1^2(v,\alpha) + I_2^2(v,\alpha)|^2 + 4|I_0(v,\alpha)\, I_2(v,\alpha) + I_1^2(v,\alpha)|^2\right\} v\, \mathrm{d}v, \tag{36}$$

and in transmission by

$$I_{\mathrm{int}} = \int_0^{\infty}\left\{\left(|I_0(v,\alpha)|^2 + 2|I_1(v,\alpha)|^2 + |I_2(v\alpha)|^2\right)^2 + 4\left(\mathrm{Re}\{I_0(v,\alpha)\, I_2^*(v,\alpha)\} + |I_1(v,\alpha)|^2\right)^2\right\} v\, \mathrm{d}v. \tag{37}$$

These expressions are shown in Fig. 13(a) for the specific case of $\alpha = 60°$. In general the curves for transmission and reflection are very similar although the sectioning in the reflection case is always slightly sharper.

In the case of imaging between crossed polars, whether

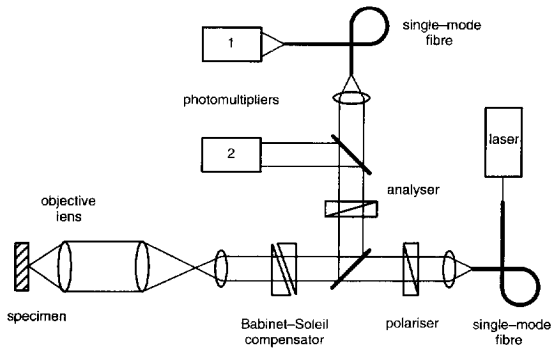

Fig. 16. Schematic diagram of the experimental arrangement.

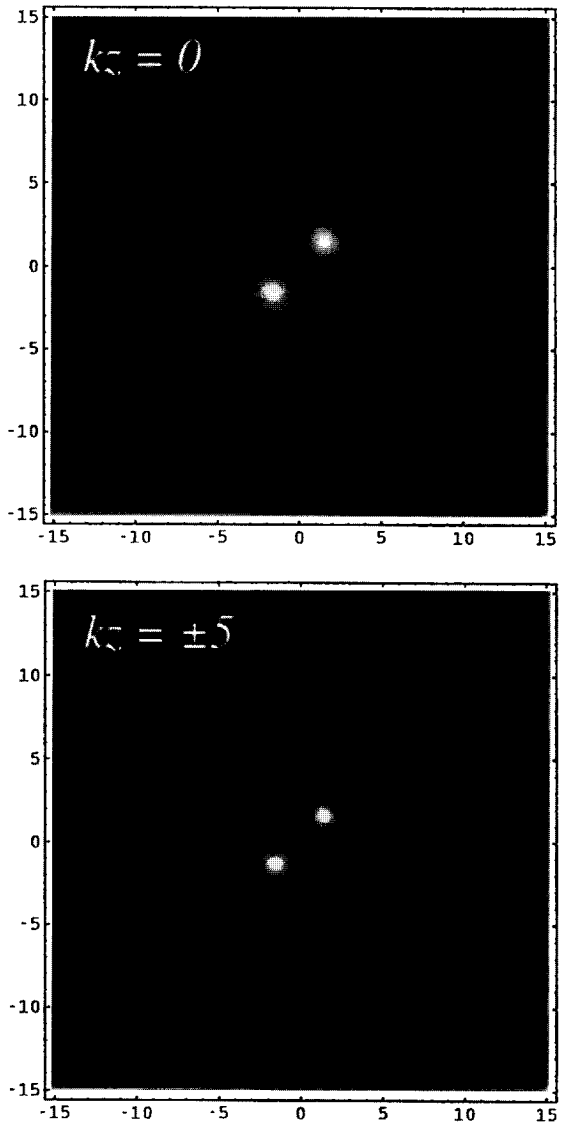

Fig. 15. The interference image between crossed linear polars for the case of $\alpha = 60°$ for zero defocus and equal and opposite defoci $kz = \pm 5$. The image area is 30 optical units square.

linear or circular polarisation is used, the integrated intensity is given by

$$I_{\text{int}}(z) = \int_0^\infty |I_0(v,\alpha)\, I_2(v,\alpha) + I_1^2(v,\alpha)|^2\, v\, \mathrm{d}v \qquad (38)$$

for a reflection system and by

$$I_{\text{int}}(z) = \int_0^\infty \left(\mathrm{Re}\{ I_0(v,\alpha)\, I_2^*(v,\alpha)\} + |I_1(v,\alpha)|^2\right)^2 v\, \mathrm{d}v \qquad (39)$$

in transmission. These functions are compared in Fig. 13(b) for the specific case of $\alpha = 60°$ which shows that the sectioning strength is, in general, different in reflection and transmission systems being poorer in reflection.

We finally return to the case of "crossed circular" polarisation, Eq. (31), and note that the phase of the image field is a function of azimuth, ϕ_s. This has implications for the form of the image in a polarisation interference microscope. In order to discuss this let us restrict ourselves to a

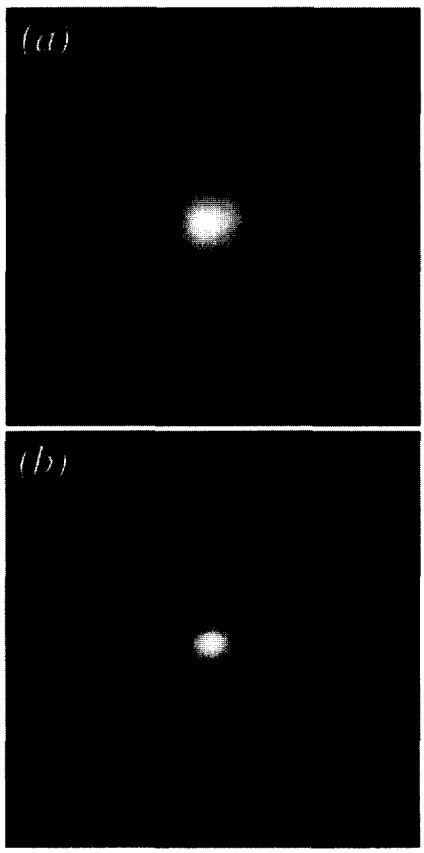

Fig. 17. The brightfield image of an InP scatterer in (a) conventional and (b) confocal microscopes. The images were obtained using a 100×1.4NA Leica Planapochromat objective. The image field is 2.0 μm square.

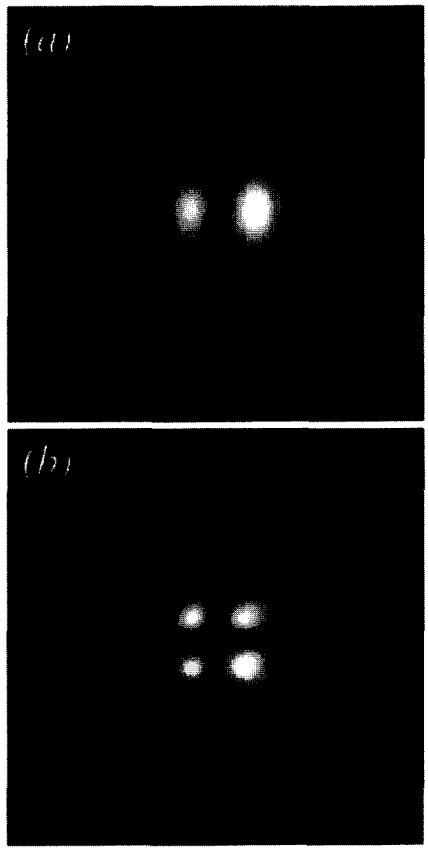

Fig. 18. The image between crossed linear polars of an InP scatterer in (a) conventional and (b) confocal microscopes. The images were obtained using a 100×1.4NA Leica planapochromat objective. The image field is 2.0 μm square.

reflection system and introduce the modulus, $f(v)$, and phase, $\phi(v)$, of $I_0(v,\alpha)\, I_2(v,\alpha) + I_1^2(v,\alpha)$ by

$$f(v)\exp \mathrm{j}\phi(v) = I_0(v,\alpha)\, I_2(v,\alpha) + I_1^2(v,\alpha). \qquad (40)$$

If we now introduce a reference beam of amplitude, r, we can write the image intensity as

$$\begin{aligned} I(v) &= |r + E_{\text{conf}}(v)|^2 = |r + f(v)\exp \mathrm{j}[2\phi_s + \phi(v)]|^2 \\ &= r^2 + 2rf(v)\cos[2\phi_s + \phi(v)] + f^2(v), \end{aligned} \qquad (41)$$

where we have assumed that r is real for simplicity. In the absence of defocus, and for small v, $\phi(v) = 0$ and hence the effect of the interference term is to impose a maximum positive contribution when $\phi_s = 0$ and π and a maximum negative contribution when $\phi_s = \pm\pi$. This is illustrated in Fig. 14 where the value of r has been chosen to make the intensity zero in the darkest region. In the presence of defocus, however, $\phi(v) \neq 0$. At a particular value of v, $\phi(v)$ is constant, and hence acts as an offset in the argument of the cosine term in Eq. (41) which causes the location of the dark and bright regions to rotate. Further since the phase, $\phi(v)$, varies with v so does the rotation of

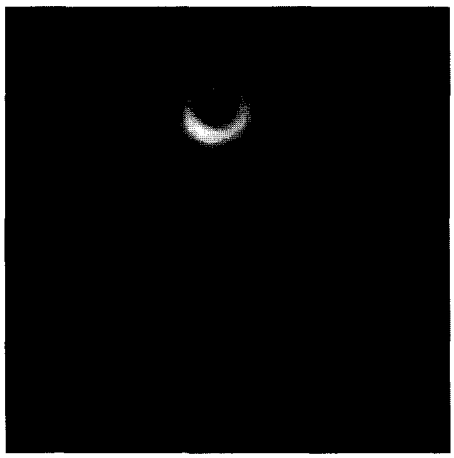

Fig. 19. The image between crossed circular polars of two scatterers on a silicon substrate in a confocal microscope. The image was obtained using a 50×0.8NA Olympus MSPlan objective. The image field is 4.4 μm square.

the dark and bright regions. This causes the image to take on a spiral like appearance, Fig. 14. We note that if the defocus is of opposite sign then $\phi(v) \rightarrow -\phi(v)$ and a spiral of opposite sense results, Fig. 14.

The behaviour in the case of crossed linear polars is quite different. In this case the confocal image field is given by Eq. (30) which leads to an interference image of the form

$$I(v) = |r + f(v)\sin 2\phi_s \exp j\phi(v)|^2 = r^2 + 2rf(v)\sin 2\phi_s \cos\phi(v) + f^2(v)\sin^2 2\phi_s. \quad (42)$$

The final term gives rise to a four leaf clover image as does the second term except here the contribution to the second and fourth quadrant is negative. This results in an interference image which is generally brighter in the first and third quadrants, Fig. 15. The effect of defocus in this case is to broaden $f(v)$ and to reduce the amplitude of the second term via $\cos\phi(v)$. Fig. 15 again illustrates the effect and emphasizes that the behaviour for positive and negative values of defocus is identical since $\cos\phi(v)$ is an even function.

3. Experimental

Fig. 16 shows a schematic of the system used to confirm these predictions. In essence it consists of a fibre optic based confocal microscope into which various polarising elements may be placed as necessary together with an extra beamsplitter to detect the conventional image via photomultiplier 2. In our experiments we used a helium neon laser and mechanical object scanning together with a variety of scatterers. In all cases the linear polariser was present to determine the input polarisation.

Our first specimen consisted of a finely ground powder

Fig. 20. Interference images between (a) crossed linear polarisation the absence of defocus. The image of an extremely weak scatterer is indicated with an arrow. (b), (c) Correspond to the case of crossed circular polars with equal and opposite defocus. The image was obtained using a 50×0.8NA Olympus MSPlan objective. The image field is 4.4 μm square.

of indium phosphide mounted on a microscope slide. We choose to image the scatterer which gave the weakest signal so as to avoid imaging large particles or aglomerations of smaller ones. Fig. 17 shows the comparison between the conventional and confocal images in the absence of any polarisation analysers. These correspond to the usual brightfield imaging and we confirm, as expected, that the resolution in the confocal image is roughly 1.4 times superior to that in the conventional image. If we now introduce a linear polar into the detection arm then the conventional and confocal images take the form shown in Fig. 18. These images exhibit the form and symmetry predicted and should be compared with Figs. 6(c) and 10.

As we have seen images obtained with linear polarisation exhibit anisotropy whereas those using circular polarisation do not. In order to demonstrate this we constructed a second specimen consisting of polystyrene spheres of 0.23 μm nominal diameter on a silicon substrate. Fig. 19 shows an image taken between crossed circular polars. In order to obtain this image the Babinet–Soleil compensator was introduced into the system. The brighter image corresponds to scattering from a polystyrene sphere whereas the weaker image is probably due to scattering from a dust particle or other impurity. The fact that the two images are identical, apart from their strength, confirms that we are imaging sub-resolution particles. The absence of signal from the planar silicon substrate illustrates the very high extinction coefficient available in confocal instrument.

We noted in Eqs. (30) and (31) that the phase of the confocal image field was very different when imaging between crossed linear and crossed circular polars. In order to demonstrate this difference we constructed a simple interference microscope by slightly uncrossing the polars. This has the effect of permitting an amount of the light reflected from the silicon substrate to act as a reference beam and to interfere with the scattered field. Fig. 20(a) shows the interference image between crossed linear polars. The symmetry is as predicted in Fig. 15 although the pattern here is rotated relative to that in the calculations. This is because the phase of the reference beam was set arbitrarily equal to zero in that case. We note both the weak and strong scatter are imaged in the same way and also that an even weaker scatter is now visible (see arrow) due to the linear imaging of weak objects in interference microscopy rather than the quadration imaging in non-interference microscopy. Finally Figs. 20(b) and 20(c) show the interference images using crossed circular polarisation. The spiral structure is clear as is the change in sense of the spiral with opposite sign of defocus, Fig. 14.

4. Conclusions

We have presented a theory of imaging in a variety of polarisation microscope geometries. The theory has been based on the ability to describe the dielectric scatterer as an electric dipole whose dipole moment is proportional to the incident electric field. Since the scatter is located in the focal region of a high numerical aperture microscope objective we have used the vector theory of Richards and Wolf [7] to describe the dipole moment. The vector nature of this theory, rather than its applicability to high apertures, is the key which permits us to analyse the imaging in conventional and confocal polarisation microscopes. In general we find that the use of linear polarisation results in asymmetric images whereas circular polarisation produces circularly symmetric images. We have also considered the effects of system defocus and here it is seen that transmission and reflection confocal systems behave in a fundamentally different manner. The defocus behaviour with linear and circular polarisation is also different and so care should be taken in interpreting polarisation images if the system is defocussed.

References

[1] P. Gay, An introduction to Crystal Optics (Longman, London, 1967).
[2] S. Inoué, Video Microscopy (Plenum, New York, 1986).
[3] M. Pluta, Advanced Light Microscopy, Vol. 3, Measuring Techniques (Elsevier, Amsterdam, 1993).
[4] T. Wilson, R. Juškaitis, J. Microsc. 179 (1995) 238.
[5] H. Kubota, S. Inoué, J. Opt. Soc. Am. 49 (1959) 191.
[6] R. Burtin, Optica Acta 3 (1956) 104.
[7] B. Richards, E. Wolf, Proc. Roy. Soc. A 253 (1959) 358.
[8] C.J.R. Sheppard, T. Wilson, Proc. Roy. Soc. A 379 (1982) 145.
[9] G. Mie, Ann. Physik 25 (1908) 377.
[10] M. Kerker, The scattering of light and other electromagnetic radiation (Academic Press, New York, 1969).
[11] M. Born, E. Wolf, Principles of Optics (Pergamon Press, Oxford, 1975).
[12] J.D. Jackson, Classical Electrodynamics (Wiley, New York, 1975).
[13] C.F. Bohren, D.R. Huffman, Absorption and Scattering of Light by Small Particles (Wiley, New York, 1983).
[14] T. Wilson, C.J.R. Sheppard, Theory and Practice of Scanning Optical Microscopy (Academic Press, London, 1984).
[15] T. Wilson, Ed., Confocal Microscopy (Academic Press, London, 1990).